Available online at www.sciencedirect.com
SCIENCE DIRECT®
Journal of Sound and Vibration 292 (2006) 59–81
JOURNAL OF SOUND AND VIBRATION
www.elsevier.com/locate/jsvi

Free vibration of an edge-cracked beam with a Dugdale–Barenblatt cohesive zone

D.A. Mendelsohn*

Department of Mechanical Engineering, The Ohio State University, Columbus, OH 43212, USA

Received 28 October 2004; received in revised form 5 July 2005; accepted 17 July 2005
Available online 26 September 2005

Abstract

This paper presents a theoretical investigation into the effect of crack-plane plasticity on the vibration of a transversely edge-cracked beam. The crack-plane is presumed to be loaded statically in either bending or shear such that Dugdale–Barenblatt type cohesive zones are activated in the crack-plane ahead of the crack tip. Then the beam undergoes small amplitude vibrations about this state. Euler–Bernoulli beam theory is used for the vibration analysis in which an infinitesimally thin beam element surrounding the crack-plane is replaced with a bending and a shear line-spring. The line-springs by nature account for the discontinuities in slope and deflection, respectively, across the crack-plane. Previous studies of the elastic problem (no cohesive zones) calculate the compliances of the line-springs from tabulated linear elastic fracture mechanics solutions and the compliances depend only on the flexural rigidity of the beam and on the crack length to beam depth ratio. Here the compliance of the line-spring for the mode loaded statically in the nonlinear range is calculated using the Boundary Element Method (BEM) in an iterative nonlinear analysis and the compliance depends nonlinearly on the load across the crack plane. This nonlinear load–deformation relation is linearized about the applied static load level, and the resulting compliance used in the vibration analysis. Among other results for mode I cohesive zones, there is a strong reduction of the fundamental frequency as both load and crack length increase and as yield strength decreases. The results show that there is some potential for designing a non-destructive material characterization technique which would use the changes in frequency to infer the properties of material behavior laws in the cohesive zone.

*Tel.: +1 614 292 2413; fax: +1 614 292 7369.
E-mail address: mendelsohn.1@osu.edu.

0022-460X/$ - see front matter © 2005 Elsevier Ltd. All rights reserved.
doi:10.1016/j.jsv.2005.07.037

1. Introduction

It is well known that the presence of cracks influences the vibrational characteristics of structures, primarily by reducing the structure's stiffness in particular modes. Natural frequency versus crack geometry relationships are of interest, for example, in the assessment of the performance integrity of cracked structures, non-destructive evaluation of the extent and location of cracking, and prediction of the resonant frequency in high-cycle fatigue. The reduction in natural frequencies caused by transverse cracks in linear elastic beams and similar thin structures have been studied extensively both theoretically and experimentally. See Refs. [1–14], the numerous references cited therein, and in particular the 1996 review by Dimarogonas [5]. A typical beam analysis involves a linear elastic frequency analysis of the vibrating beam, modeled by Euler–Bernoulli or some higher order beam theory on either side of the (infinitesimally thin) crack plane along with one of various models for representing the localized increased compliance of the beam in the neighborhood of the crack plane caused by the presence of the crack. Theoretical knowledge of the dependence of frequency reduction on crack length and position then provides a technique for locating and sizing a crack in a beam from experimentally measured frequency spectra.

The majority of the work cited above in vibration signatures of cracked and damaged structures has been linear, however there has been a reasonable effort to understand the breathing crack nonlinearity which manifests itself in any physical situation where the crack faces are not prevented from opening and closing tight during the vibration. This phenomenon, when allowed to occur, results in higher harmonics generated through the coupling of the bending vibrations with longitudinal motions in the direction of the opening and closing [5,15–18]. The crack face contact also decreases the compliance and, hence, lessen the reduction in frequency compared to an analysis that ignores the closure portions of the vibration cycle.

This nonlinear work and almost all of the work cited as background to the present study is related to non-destructive evaluation of cracked civil and mechanical structures. In contrast, the intent in the present line of investigation is to use the frequency spectra of small laboratory beam specimens of ductile materials (or simple composite beams with a single ductile interface) to investigate material behavior near the crack tip. This of course requires both the appropriate modeling and analysis and the accompanying measurements. This paper contains the first of the modeling and analysis studies. The eventual purpose is not flaw identification, but rather the goal is to infer the controlling parameters in a crack plane cohesive traction–displacement relationship (model) from frequency measurements. Because of this, the present line of investigation is significantly different in two ways from all of the previous structural vibration analyses, measurements, and inverse techniques for sizing and locating cracks, some of which are referenced above. First, the vibration is envisioned to take place while the specimen is subjected to a large static bending moment [up to as much as 60% of the plastic limit moment for the uncracked beam] and second, the crack length to beam depth ratio must be intentionally quite large in order to obtain a reasonable length cohesive zone and a strong effect on the frequency spectrum. In contrast, a non-destructive testing technique for detecting sub-critical size flaws to avoid the failure of civil or mechanical structures during service have not been applied to situations with such large crack length to beam depth ratios or such severe static pre-loading conditions. However, the calculations here are in the context of a laboratory non-destructive testing technique

intended for material evaluation and characterization, in which, as described above, such crack geometries and loading conditions are desirable.

Also, the present paper is only an introductory theoretical investigation. While, experiments are planned for the future under these conditions, the models in the present analysis have not been verified yet for a particular material in this setting. Future work will also include calculations for more complex cohesive laws to be tested against experimental results, and appropriate models chosen based on the ability to obtain correlations between frequency measurements and predictions. It is possible that experimental verification of cohesive laws for a few test materials by some means other than frequency spectra will also be needed for a complete verification. There is a large body of experimental frequency measurement work on the linear problem that has been tied first to linear elastic fracture mechanics models to create techniques for determining crack tip fields, and later for locating and sizing small cracks and some of that literature is cited above, see e.g. the review in Ref. [5]. However, there is not a single experiment of which the author is aware that is like the one envisioned with very large static preloads, long cracks, and finite length cohesive zones. Hence there are no comparisons to experimental data in this paper.

Assuming Euler–Bernoulli beam theory, uniform rectangular beams, classical boundary conditions at the ends of the beam and linear line-spring representations for the crack planes, the frequency determinant can be derived easily in closed form or numerically in terms of the bending and shear compliances across multiple crack planes. These compliances are derivable from well-tabulated two-dimensional linear elastic fracture mechanics calculations for the stress intensity factors or crack face displacements of transversely cracked beams [9]. In this linear setting the line-spring compliances depend only on the crack length, beam depth and Poisson's ratio and are independent of the magnitude of the load (bending moment or shear force across the crack plane) because the spring displacement depends linearly on load. The purpose of the present analysis is to explore the effect of localized material nonlinearities in the crack plane which cause the line-spring compliances to depend on the crack-plane load (bending moment or shear force) magnitude on the frequency response in an otherwise linear vibration analysis. The potential for the use of these results for extracting the crack plane yield stress at a static pre-load and a known crack length and location from the measurements of the natural frequencies and mode-shape.

Many materials exhibit a region of plastic behavior that is limited to a thin planar zone ahead of the crack edge, often referred to as a cohesive zone. The thickness is either taken to be on the order of some micro-structural dimension, or, more often than not, in a macroscopic calculation the thickness is assumed negligible. The other distinguishing property of a cohesive zone is that although very thin, it undergoes stretching (normal to the crack plane) or shearing (of one planar surface with respect to the other) when the crack is loaded in Mode I or II, respectively. This imparts a discontinuity in the normal and/or tangential displacements in the surrounding material on opposite faces of the cohesive zone, just as it occurs across opposing faces of the crack, except that this discontinuity represents plastic stretching or shearing of intact material as opposed to separation or sliding of opposing non-contacting crack surfaces. If the surrounding material remains elastic, cracked bodies with cohesive zones can be modeled with elastic boundary value problems in which all nonlinear cohesive zone behavior appears only in the boundary conditions on stress and displacement on opposing sides of the planar cohesive zone. From the point of view of the cracked beam vibration problem the essential effects are twofold. First, the crack length is effectively increased, thus increasing the compliance and the reduction in natural frequencies

compared to those of the effectively shorter elastic crack. Second and more importantly, the bending or shear compliance depends nonlinearly on the crack-plane bending moment or shear force, respectively. Thus, the compliance changes during a cycle of vibration, requiring a linearization procedure for estimating the effective vibrational compliance.

The original cohesive zone models due almost simultaneously to Dugdale and Barenblatt assumed that in mode I, independent of the amount of cohesive zone stretching, the tensile stress across the cohesive zone is everywhere equal to the yield stress in tension of the material. However, there is much evidence and theoretical justification for the notion that as the plastic stretching or shearing approaches a critical value the stress necessary to cause the plasticity decreases to zero at the critical value which coincides with unstable crack growth. The present analysis is limited to the simpler, albeit less realistic, Dugdale–Barenblatt model which does not allow for softening. Softening cohesive zones will be treated in subsequent work.

Section 2 contains the framework for the nonlinear line-spring model in both the beam vibration and fracture mechanics settings. This section results in an effective crack-plane compliance for use in the vibration analysis, described in Section 3, which depends on the J-integral for a cracked beam segment with a cohesive zone, the calculation of which is described in Section 4. Section 5 presents the numerical results for the compliances as a function of load, crack length and cohesive zone yield strength. Section 6 presents the resulting natural frequencies and some concluding remarks are made in Section 7.

2. Crack-plane compliance and nonlinear cracked beam response

The effect of the crack on the vibration of the rest of the beam will be modeled by a line-spring, i.e. the crack plane is assumed to divide the beam into two regions which interact across the crack plane through zero width bending and shear springs which allow discontinuities in deflection and slope. To obtain the stiffnesses (or their reciprocal, the compliance) of these crack plane springs a representative cracked beam element is analyzed using static 2D fracture mechanics as described below in Section 4. Figs. 1a and b show such representative cracked beam elements and serve to illustrate all of the quantities which appear in the two line-spring relations. The discontinuities in slope $[\Theta]$ and deflection $[W]$ across the crack plane are assumed to be functions of the crack plane bending moment M and shear force Q, respectively through the compliances λ_θ and λ_W. Let the

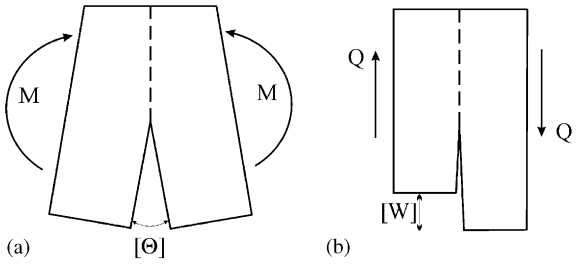

Fig. 1. Cracked beam elements: (a) Mode I crack plane bending moment and discontinuity in slope, $P = M$, $\Delta = [\Theta]$, $[\Theta] = \lambda_\theta M$. (b) Mode II crack plane shear force and discontinuity in displacement, $P = Q$, $\Delta = [W]$, $[W] = \lambda_W Q$. The dashed line represents the ligament (intact part of the crack plane).

generalized load be P and the generalized displacement Δ be the kinematic discontinuity across the crack plane. Then the generalized line-spring relation can be written in terms of the generalized compliance λ and the bending and shear mode spring relations are given as separate cases:

$$\Delta = \lambda P, \tag{1}$$

$$\begin{aligned} &\textit{Bending}: \quad \Delta = [\Theta] = W_1' - W_2', \quad \lambda = -\lambda_\theta, \quad P = M, \\ &\textit{Shear}: \quad \Delta = [W] = W_1 - W_2, \quad \lambda = \lambda_W, \quad P = Q. \end{aligned} \tag{2a, b}$$

The $W_i = W_i(x)$ are the x-dependences of the deflections $w_i(x,t)$ $(i = 1, 2)$ in the two parts of the beam, and primes denote differentiation with respect to x. This modification of the original line-spring concept [19] is used, e.g., in Ref. [9] to analyze the vibration of an elastic cracked beam in the absence of a crack plane cohesive zone. The compliance in this case is a function of the beam properties and the crack length to beam depth ratio only, Eq. (1) is a linear relationship, and there are no difficulties in carrying out a traditional linear beam vibration analysis for a two part beam connected by linear springs.

Referring again to Fig. 1, it is seen that for a crack of length less than or equal to half the depth of the beam, bending causes a tensile mode I stress state at the crack tip and transverse shear loading causes a mode II state. If either mode loading is sufficient to cause a cohesive zone to be activated during vibration then the compliance depends on the load nonlinearly and the load–displacement relationship is no longer linear. Hence, if there is cohesive behavior, since the crack-plane loading varies during a vibration cycle, the compliance is also a function of time. This violates the separable, time-harmonic solution form for $w(x,t)$ assumed in traditional linear vibration analysis, which requires the compliances to be constant in time. Hence in order to capture exactly the interaction between compliance and load during a cycle of vibration a fully transient solution must be carried out both for the beam vibrations and for the cracked compliance calculation, which would require iteration at each time-step to satisfy Eq. (1).

However, if, as envisioned in the present situation, the beam is subjected to a static pre-load causing cohesive behavior, and then allowed to undergo small amplitude vibration about this state, then the nonlinear load–displacement relation can be linearized about the static operating point. This is outlined in Fig. 2, which shows a softening nonlinear load–displacement relation and a local tangent line at the operating point along which the cracked beam element is assumed to load and unload during a vibration cycle. The effective dynamic stiffness is the slope of the tangent line at the operating point, as opposed to the stiffness which is the slope of the line from (0, 0) to (P_0, Δ_0). For the mode in the linear range, the effective and actual compliance are the same. Noting Eq. (1) then the effective compliance at any load P and corresponding displacement Δ is given by

$$\lambda_{\text{eff}}(P,a) = \frac{\partial \Delta}{\partial P} = \lambda(P,a) + P\frac{\partial \lambda(P,a)}{\partial P}. \tag{3}$$

Because of unresolved conceptual difficulties with a mixed-mode planar cohesive zone, it is assumed that in this first study only one mode is loaded statically into the nonlinear range at any time, the cohesive zone is purely that mode, and the other mode is in the elastic range. In other

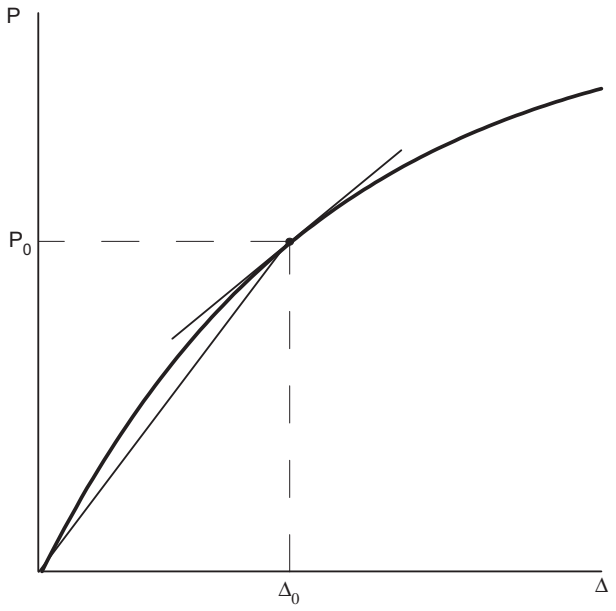

Fig. 2. A softening nonlinear cracked beam element response curve at some fixed crack length, a. The effective linearized stiffness (inverse of the effective compliance) used in the vibration analysis is the slope of the local tangent line to the curve, whereas the slope of the line from the origin to a point on the curve is the inverse of the compliance itself.

words, if the static loading is, for example, in bending (mode I), then the plastic $\lambda_\theta = \lambda_{\theta\text{eff}}$ is found from Eq. (3) and the elastic λ_W may be found from the results in Yokoyama or by using the present analysis without a cohesive zone.

It now remains to determine $\lambda(P, a)$ for the cracked beam element with a cohesive zone. This is done by relating it to the J-integral through an energy argument applied to a cracked beam element. The strain energy release rate of a cracked body is defined to be the amount of strain energy stored in the cracked body available to create new crack surface per unit area of crack surface created and is given by [20]

$$G(P,a) = -\frac{1}{b}\frac{\mathrm{d}\Pi(P,a)}{\mathrm{d}a}, \tag{4}$$

where b is the out of plane thickness of the cracked body, a is a coordinate measuring crack length and $\Pi(P, a)$ is the total strain energy stored in the cracked body. Assuming the only external load on the cracked body which does work is the load P, and also assuming load control, the stored strain energy is minus the work done by the load through the displacement. This and the use of Eqs. (1) and (4) and the equivalence of the strain energy release rate and the J-integral defined in Section 4, gives

$$\Pi(P,a) = -\int_0^P \Delta(P,a)\,\mathrm{d}P = -\int_0^P \lambda(P,a)P\,\mathrm{d}P$$

$$\Rightarrow J(P,a) = G(P,a) = \frac{1}{b}\int_0^P \frac{\partial\lambda(P,a)}{\partial a} P\,\mathrm{d}P$$

$$\Rightarrow \lambda(P,a) = \frac{b}{P}\int_0^a \frac{\partial J(P,a)}{\partial P}\,\mathrm{d}a. \tag{5a–c}$$

In this two-dimensional setting, J is really a function of the load per unit thickness out-of-plane, $\bar{P} = P/b$, and not the load itself. Also in this geometry, J is a function of crack length to depth ratio a/d and not the crack length itself. Hence the generalized compliance may be rewritten as follows:

$$\lambda(P,a) = \lambda(\bar{P},a/d) = \frac{d}{b}\frac{1}{\bar{P}}\int_0^{a/d} \frac{\partial J(\bar{P},a/d)}{\partial \bar{P}}\,\mathrm{d}(a/d). \tag{6}$$

Substituting this $\lambda(P, a)$ into Eq. (3) gives the desired effective compliance to be used below in the beam vibration analysis.

3. Beam vibrations with a line-spring and the frequency determinant

The beam shown in Fig. 3 is cracked along the plane $x = c$ from $y = -d/2$ to $y = -d/2 + a$. The beam is divided into regions 1: $0<x<c$ and 2: $c<x<L$ in which the equations of motion of Euler–Bernoulli beam theory in the absence of transverse loading and rotary inertia apply:

$$EI\frac{\partial^4 w(x,t)}{\partial x^4} + \rho A\frac{\partial^2 w(x,t)}{\partial t^2} = 0. \tag{7}$$

The two regions of the beam interact through bending and shear line springs with compliances λ_θ and λ_W. If the static loading is, for example, in bending, then $\lambda_\theta = \lambda_{\theta\mathrm{eff}}$ as defined above in Eqs. (3) and (6), and $\lambda_W = \lambda_{W\mathrm{elastic}}$, which may be found from the formulas in Yokoyama or by using the present analysis without a cohesive zone. Eq. (7) assumes a positive upward deflection $w(x, t)$ and the convention that concave up corresponds to positive curvature. The sign convention on the bending moment is such that positive bending moments $M(x, t)$ cause positive curvature and positive shear $Q(x, t)$ is down on a cross-section facing to the right. Considering vibratory motion, let the deflection be of the form $w(x, t) = W(x)\sin(\omega t)$. Then the sign conventions

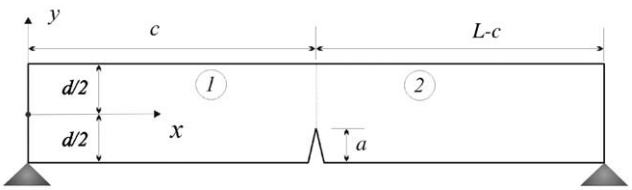

Fig. 3. Simply supported cracked beam geometry for vibration analysis. The beam depth and length are d and L, respectively. The crack length and position are a and c, respectively. The origin of the coordinate system is at the left end of the beam as shown.

stated imply:

$$Q(x,t) = EIW'''(x)\sin(\omega t),$$
$$M(x,t) = EIW''(x)\sin(\omega t),$$
$$Q(x,t) = \frac{\partial M(x,t)}{\partial x}. \tag{8a–c}$$

The general solutions of Eq. (7) for each region are written below in terms of the non-dimensional wavenumber κ and position coordinate $\xi = x/L$

$$W_1(\xi) = c_1\ \sin(\kappa\xi) + c_2\ \cos(\kappa\xi) + c_3\ \sinh(\kappa\xi) + c_4\ \cosh(\kappa\xi), \quad \xi < \beta,$$
$$W_2(\xi) = c_5\ \sin(\kappa\xi) + c_6\ \cos(\kappa\xi) + c_7\ \sinh(\kappa\xi) + c_8\ \cosh(\kappa\xi), \quad \xi > \beta, \tag{9a, b}$$

where the non-dimensional wavenumber is given by

$$\kappa^2 = \omega L^2\sqrt{\frac{\rho A}{EI}} \tag{10}$$

in terms of the frequency, ω; the flexural rigidity, EI; the mass per unit volume, ρ; the length of the beam L, and the uniform cross-sectional area $A = b \times d$, where b is the beam thickness and d is the depth of the beam. The constant $\beta = c/L$ is the non-dimensional position of the crack, see Fig. 3. While the following is for the simply supported beam, other boundary conditions may be treated with the same technique. The simply supported conditions at each end eliminate four of the eight constants:

$$W_1(0) = W_1''(0) = 0 \Rightarrow c_2 = c_4 = 0,$$
$$W_2(1) = W_2''(1) = 0 \Rightarrow c_6 = -c_5\ \tan(\kappa), c_8 = -c_7\ \tanh(\kappa). \tag{11a, b}$$

The remaining four boundary conditions are across the crack plane $\xi = \beta$. The first two are continuity of bending moment and shear force across the crack plane and the third and fourth conditions express the line-spring model, Eqs. (1) and (2), for the crack plane.

$$W_2''(\kappa\beta) = W_1''(\kappa\beta),$$
$$W_2'''(\kappa\beta) = W_1'''(\kappa\beta),$$
$$W_1'(\kappa\beta) - W_2'(\kappa\beta) = -\lambda_\theta EIW_1''(\kappa\beta),$$
$$W_1(\kappa\beta) - W_2(\kappa\beta) = \lambda_W EIW_1'''(\kappa\beta). \tag{12a–d}$$

Substitution of the expressions for c_6 and c_8 from Eq. (11b) and applying these four boundary conditions yields four linear non-dimensional homogenous equations in the remaining constants c_1, c_3, c_5 and c_7. The frequency equation is thus given by

$$D = \det\begin{bmatrix} -\sin(\kappa\beta) & \sinh(\kappa\beta) & \sin(\kappa\beta) - \cos(\kappa\beta)\tan(\kappa) & -\sinh(\kappa\beta) + \cosh(\kappa\beta)\tanh(\kappa) \\ -\cos(\kappa\beta) & \cosh(\kappa\beta) & \cos(\kappa\beta) + \sin(\kappa\beta)\tan(\kappa) & -\cosh(\kappa\beta) + \sinh(\kappa\beta)\tanh(\kappa) \\ \sin(\kappa\beta) + \bar{\lambda}_W\kappa^3\cos(\kappa\beta) & \sinh(\kappa\beta) - \bar{\lambda}_W\kappa^3\cosh(\kappa\beta) & -\sin(\kappa\beta) + \cos(\kappa\beta)\tan(\kappa) & -\sinh(\kappa\beta) + \cosh(\kappa\beta)\tanh(\kappa) \\ \cos(\kappa\beta) - \bar{\lambda}_\theta\kappa\sin(\kappa\beta) & \cosh(\kappa\beta) - \bar{\lambda}_\theta\kappa\sinh(\kappa\beta) & -\cos(\kappa\beta) - \sin(\kappa\beta)\tan(\kappa) & -\cosh(\kappa\beta) + \sinh(\kappa\beta)\tanh(\kappa) \end{bmatrix} = 0. \tag{13}$$

The determinant D is a function only of κ, $\beta = c/L$ and the non-dimensional compliances:

$$\bar{\lambda}_\theta = \frac{\lambda_\theta EI}{L}, \qquad \bar{\lambda}_W = \frac{\lambda_W EI}{L^3}. \tag{14a,b}$$

For given β, $\bar{\lambda}_\theta$, and $\bar{\lambda}_W$ the determinant is expanded symbolically, set equal to zero and the first three roots for κ are found numerically after obtaining search ranges for the roots graphically. The corresponding natural frequencies can then be found from Eq. (10). The mode shapes may also be found then from Eqs. (9), (11) and (13).

4. *J*-integral reduction and BEM calculation of crack tip displacements

The J-integral is a path independent line integral surrounding the crack tip and is defined as [20]

$$J = \oint_\Gamma \left[U\,\mathrm{d}x_1 - T_1 \frac{\partial u_1}{\partial x_2}\,\mathrm{d}s - T_2 \frac{\partial u_2}{\partial x_2}\,\mathrm{d}s \right], \tag{15}$$

where the strain energy density U and the traction and displacement vectors (T_1, T_2) and (u_1, u_2) are functions of the coordinates (x_1, x_2) with origin and orientation such that $x_1 = 0$ is the crack plane. In this section the dependence of all quantities on load and crack length has been suppressed. The path Γ may be any counterclockwise path in the (x_1, x_2) plane which

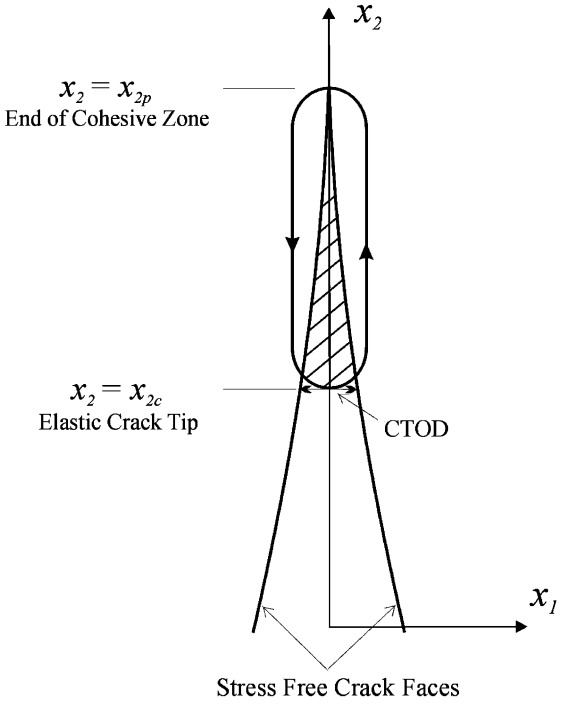

Fig. 4. A mode I cohesive zone. Hash marks denote plastically deformed material in the zone. The crack tip opening displacement (CTOD) is shown, as is the path for the J-integral.

circumscribes the crack tip and ds is an increment of length along the path. Fig. 4 shows a schematic of a mode I cohesive zone and the path chosen in this analysis. The position of the elastic crack tip is x_{2c} and x_{2p} is the a priori unknown position of the end of the cohesive zone. As Γ shrinks around the cohesive zone it becomes, in the limit, the two paths: $\{x_1 = 0+$, from $x_2 = x_{2c}$ to $x_2 = x_{2p}\}$, $\{x_1 = 0-$, from $x_2 = x_{2p}$ to $x_2 = x_{2c}\}$. On these paths $\mathrm{d}s = +\mathrm{d}x_2$ and $-\mathrm{d}x_2$, respectively, and $\mathrm{d}x_1 = 0$. Continuity of stress across the cohesive zone requires $T_{i-} = -T_{i+}$ $(i = 1, 2)$. Hence the J-integral reduces to

$$J = -\int_{x_{2c}}^{x_{2p}} \left[T_{1+} \frac{\partial [u_1]}{\partial x_2} + T_{2+} \frac{\partial [u_2]}{\partial x_2} \right] \mathrm{d}x_2, \tag{16}$$

where the $[u_i](x_2) \equiv [u_i(x_1, x_2)]_{x_1=0+} - [u_i(x_1, x_2)]_{x_1=0-}$ $(i = 1, 2)$ are the jumps in displacement across the crack plane which represent plastic stretching in the cohesive zone. Recalling that the analysis is limited to the case of a single mode cohesive zone, one or the other of these jumps is zero. Each mode's separate J-integral is then

$$J_I = -\int_{x_{2c}}^{x_{2p}} T_{1+} \frac{\partial [u_1]}{\partial x_2} \, \mathrm{d}x_2,$$
$$J_{II} = -\int_{x_{2c}}^{x_{2p}} T_{2+} \frac{\partial [u_2]}{\partial x_2} \, \mathrm{d}x_2. \tag{17a, b}$$

Eqs. (17a,b) are valid for any cohesive law which relates the traction to the displacement jump. The original implementation of a narrow strip cohesive zone ahead of the crack tip is due to both Dugdale [21] and Barenblatt [22], who assumed the traction is equal to the yield stress everywhere in the cohesive zone and found the length of the zone by setting the stress intensity factor at it's end equal to zero. More realistic cohesive laws which reflect many materials' softening behavior are available in the literature, some of which will be considered in later work. Only the Dugdale–Barenblatt model is used here. In that case the integrals in Eq. (17a,b) can be evaluated in closed form:

$$J_I = -\sigma_Y \left[[u_1](x_{2p}) - [u_1](x_{2c}) \right] = \sigma_Y [u_1](x_{2c}) = \sigma_Y \mathrm{CTOD},$$
$$J_{II} = -\tau_Y \left[[u_2](x_{2p}) - [u_2](x_{2c}) \right] = \tau_Y [u_2](x_{2c}) = \tau_Y \mathrm{CTSD}, \tag{17c, d}$$

where σ_Y and τ_Y are the yield stress in tension and shear, respectively, of the material, and CTOD and CTSD stand for crack tip opening displacement and crack tip sliding displacement, respectively. Hence, the nonlinear J-integral evaluation for a Dugdale–Barenblatt cohesive zone reduces to finding the CTOD or CTSD. This is done using the Boundary Element Method (BEM).

The BEM model for a cracked beam element subjected to either pure bending or pure shear causing, respectively, a pure mode I or pure mode II stress-state at the crack tip is shown in Fig. 5. To obtain the bending (mode I) case couples are applied to the left end and right ends of the beam (force pairs T_{I}). To obtain the shear (mode II) case the four vertical loads are placed so that the two inner loads (T_{IIA}), which are equidistant from the crack plane, $x_1 = 0$, create a couple equal and opposite to the one created by the outer loads (T_{IIB}), which are also equidistant from the crack plane. Since the BEM analysis is two-dimensional plane stress, the crack-plane bending moment caused by the couples of horizontal forces is really a bending moment per unit thickness, and the crack-plane shear caused by the vertical load arrangement is a shear force per unit

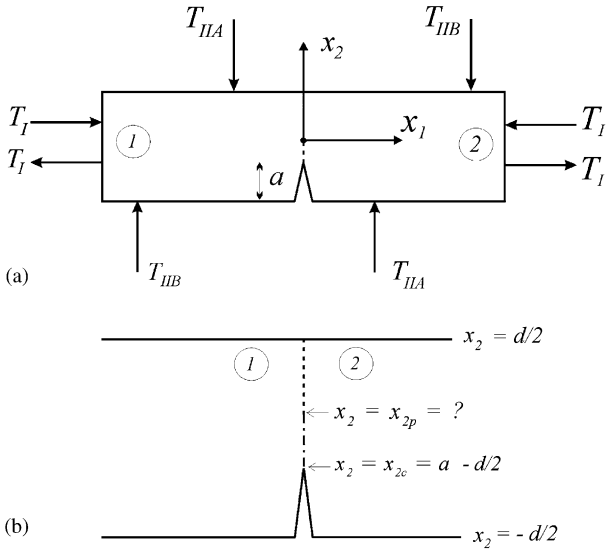

Fig. 5. (a) BEM model for the cracked beam element used for calculation of CTOD or CTSD. Origin of coordinate system is chosen in the center of the model: $x_2 = \pm d/2$ are the top and bottom of the beam and $x_2 = 0$ is the midplane. (b) Detail of crack plane boundary between two BEM regions showing the three portions of the boundary: open crack, cohesive zone (dash-dot) and bonded ligament (dash).

thickness. Recall that the J-integral and the resulting compliance are to be used in the context of the cracked beam elements in Fig. 1 which are meant to include the local crack effects only. Hence the BEM model in Fig. 5a is taken long enough in the x_1 direction so that the results are independent of the length of the model and represent crack response only. The origin of the coordinate system is midway through the depth of the model and in the crack plane. The boundaries Γ_1 and Γ_2 of regions 1 and 2 are mirror images of each other and each consist of four line segments, one of which is the shared crack plane boundary. All boundary segments are discretized into constant and equal length elements, over which tractions and displacements are assumed constant. The direct form of the two 2D BEM is used here, see Refs. [23,24] for details. The boundary conditions and iterative solution method are described next.

In the bending/mode I load arrangement only the horizontal force couples in Fig. 5a are acting. The boundary conditions on the four loaded elements on the right and left end of the beam are $(T_1, T_2) = (\pm T_I, 0)$, where the plus sign is for the upper right and lower left load elements and the minus sign is for the upper left and lower right load elements. The resultant crack plane shear force is zero and the resultant crack plane bending moment per unit thickness, $\bar{M} = M/b$, is the product of the traction T_I, the element length, and the distance between the nodes of the loaded elements.

In the shear/mode II load arrangement only the vertical force couples in Fig. 5a are applied. The traction boundary conditions on the two inner loaded elements are $(T_1, T_2) = (0, \pm T_{IIA})$, where the plus sign is for the lower element and the minus sign is for the upper element. Similarly, the boundary conditions on the two outer loaded elements are $(T_1, T_2) = (0, \pm T_{IIB})$. The resultant

crack plane bending moment is zero and the resultant crack plane shear force per unit thickness, $\bar{Q} = Q/b$, is minus the product of the difference in tractions ($T_{IIA} - T_{IIB}$) and the element length.

Boundary conditions for all unloaded elements on non-crack-plane boundaries are stress free, i.e. zero traction, $(T_1, T_2) = (0, 0)$. Referring to Figs. 4 and 5b, the boundary conditions on the two stress free crack faces are zero traction and the normal and tangential displacements on each of the faces are unknown. Discontinuities across the crack plane represent relative crack opening or crack sliding displacements. In a Mode I (II) cohesive zone the normal (shear) stress is equal to the yield stress σ_Y (τ_Y), the shear (normal) stress is zero, stress is continuous across the cohesive zone, and the normal and tangential displacements on each of the two sides of the cohesive zone (limits from the left and right) faces are unknown. Discontinuities in displacement across the cohesive zone represent plastic stretching. In the ligament, from the end of the cohesive zone to the top of the beam, continuity of normal and tangential stresses and displacements is imposed.

While the material remains elastic everywhere inside both BEM boundaries, the problem is nonlinear due to the inequality constraints which determine the unknown position of the end of the cohesive zone, x_{2p}. The first constraint is that in the cohesive zone and the crack the jump in displacements is always of the same sign and consistent with the direction of the applied loading.

$$-\frac{d}{2} < x_2 < x_{2p}, \quad \textit{Mode I} : [u_1] = (u_{1+} - u_{1-}) > 0, \quad \textit{Mode II} : [u_2] = (u_{2+} - u_{2-}) > 0. \tag{18}$$

The plus or minus in the subscript refer to evaluation at $x_1 = 0\pm$. The second constraint is that in the ligament the traction corresponding to the loading mode cannot exceed the appropriate yield stress.

$$x_{2p} < x_2 < \frac{d}{2}, \quad \textit{Mode I} : |T_{1\pm}| < \sigma_Y, \quad \textit{Mode II} : |T_{2\pm}| < \tau_Y. \tag{19}$$

If the first guess for the length of the cohesive zone is smaller than the correct value, then the stress constraint in the ligament will be violated, and if it is too large, then the displacement jump constraint will be violated. In practice, if this constraint is violated, it is always violated for some portion of the crack adjacent to the crack tip. An automatic iterative scheme was developed based on these constraints. Since calculations are done repeatedly over a slowly varying range of crack lengths, applied loads, and yield strength values, once a few calculations are made in a parameter sweep, the previous value of the length of the cohesive zone is used as a first guess for the next calculation. This usually results in only two or three iterations. As stated above and in Eq. (17) the only pertinent output from the BEM model is the CTOD in the mode I case and the CTSD in the mode II case. Since the crack tip lies at the boundary between two elements the crack tip displacement is found by averaging the values for the two elements adjacent to the crack tip; one in the cohesive zone and one in the open crack.

5. Cohesive and elastic compliance calculation

Calculations were performed for two loading situations. In the first the static loading in the nonlinear range is in bending (Mode I) and the plastic effective compliance is calculated using the CTOD calculated from BEM model in bending and the crack shear response (Mode II) is elastic

as in Yokoyama. In the second loading situation the static loading in the nonlinear range is shear (Mode II) and the plastic effective compliance is calculated using the CTSD calculated from BEM model in shear and the crack bending response (Mode I) is elastic as in Yokoyama. The latter mode II plastic results are qualitatively similar to the mode I plastic results and hence only the mode I plastic results are presented here.

In all calculations Young's modulus, Poisson's ratio and beam depth are taken to be $E = 72.8\,\text{GPa}$, $v = 0.3$ and $d = 1.25\,\text{cm}$. The beam length does not appear in the BEM formulation or in the calculation of the compliance λ_θ, through Eqs. (3) and (6), but it does appear in the definition of the non-dimensional compliances $\bar{\lambda}_\theta$ in Eq. (14a) and hence influences the frequency determinant D in Eq. (13). Results are shown for only one value of beam depth to length ratio length: $d/L = 0.1$.

In the parameter study performed, the yield stress σ_Y was varied in the range 50–100 MPa, crack lengths ranged from $a/d = 0.06$ to 0.50, and the applied static moment per unit thickness $\bar{M}$ ranged from .75 to 1.5 kN. A load of $\bar{M} = 1.5\,\text{kN}$ was sufficient to cause a cohesive zone of reasonable length at all crack lengths and yield stresses used. At each value of yield stress a matrix of $J_I(\bar{M}, a/d)$ values is calculated from Eq. (17c) using the CTOD from the BEM calculation. The dependence of the J_I both on load at fixed crack length as well as on crack length at fixed load are approximated by polynomial fits for use in the compliance calculation. Typical results for $J_I(\bar{M}, a/d)$ versus $\bar{M}$ for various a/d are shown in Fig. 6a, while Fig. 6b shows the partial of $J_I(\bar{M}, a/d)$ with respect to $\bar{M}$ versus a/d for various $\bar{M}$. While the dependence on $\bar{M}$ is similar the J values in Fig. 6a are always larger than those for the crack without the cohesive zone.

The bending compliance λ_θ is found from Eq. (6) with $\bar{P} = \bar{M}$ and the effective bending compliance $\lambda_{\theta\text{eff}}$ is calculated from Eq. (3) with $\bar{P} = \bar{M}$. Finally the effective non-dimensional compliance $\bar{\lambda}_{\theta\text{eff}}$, which appears in the frequency equation (13), is calculated using Eq. (14a). The moment of inertia of the assumed rectangular beam cross-section $b \times d$ which appears in Eq. (10b) is $I = bd^3/12$, but it should be noted that $\bar{\lambda}_{\theta\text{eff}}$ is independent of beam thickness b [see Eq. (14) and the definition of $\bar{P}$].

Fig. 7a shows plots of $\bar{\lambda}_{\theta\text{eff}}$ versus yield stress in the cohesive zone at four values of the applied moment ($\bar{M} = 0.75, 1.0, 1.25, 1.5\,\text{kN}$) at the crack length $a/d = 0.46$. Fig. 7b shows plots of $\bar{\lambda}_{\theta\text{eff}}$ versus the yield stress at three values of crack-length to depth ratio ($a/d = 0.42, 0.46, 0.50$) at the applied moment $\bar{M} = 1\,\text{kN}$. The results in Figs. 7a and b are intuitive in that the compliance decreases as the yield strength increases and makes the cracked beam element harder to bend, while the compliance increases with increasing load or relative crack length, both of which make the cracked section easier to bend.

6. Natural frequencies

Observing the determinant D in Eq. (13) for a simply supported beam of length L and depth d, the natural frequencies for the cracked beam depend only on the relative crack position $\beta = c/L$ and the non-dimensional bending and shear compliances just discussed. In all cases here the crack is at the midspan, $\beta = \frac{1}{2}$. With regard to the compliances, two different problems are given below: (1) the *elastic* problem with a crack of length a without a cohesive zone [$\bar{\lambda}_\theta = (\bar{\lambda}_\theta)_{\text{elastic}}$ and

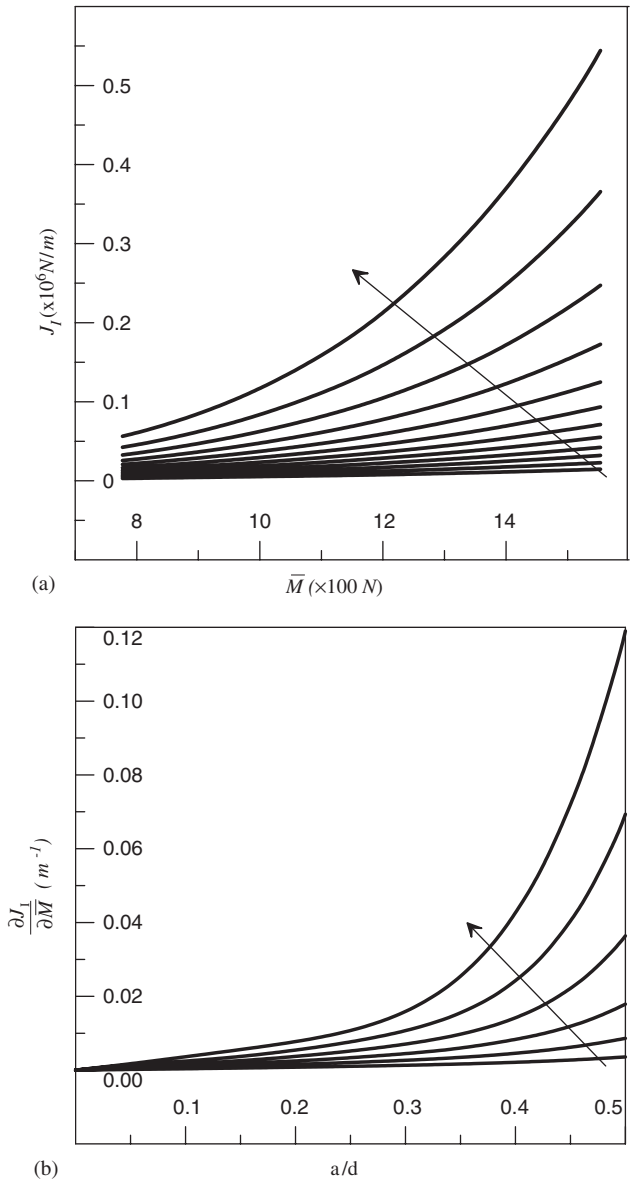

Fig. 6. (a) Typical results for the mode I J-integral versus applied moment per unit thickness for crack length to depth ratios (a/d) ranging from 0.06 to 0.50 in intervals of 0.04. The arrow indicates increasing a/d. (b) Typical results for the derivative of the J-integral with respect to applied moment per unit thickness versus crack length to depth ratio for values of applied moment per unit thickness ranging from 0.250 to 1.50 kN in intervals of 0.250 kN. The arrow indicates increasing moment.

$\bar{\lambda}_W = (\bar{\lambda}_W)_{\text{elastic}}$] and (2) the *plastic mode I* problem with a crack of length a with a cohesive zone loaded statically in mode I [$\bar{\lambda}_\theta = \bar{\lambda}_{\theta\text{eff}}$ and $\bar{\lambda}_W = (\bar{\lambda}_W)_{\text{elastic}}$]. Results for the *plastic mode II* problem are not presented here. The effective compliances for the *plastic mode I* problem are in Fig. 7. For

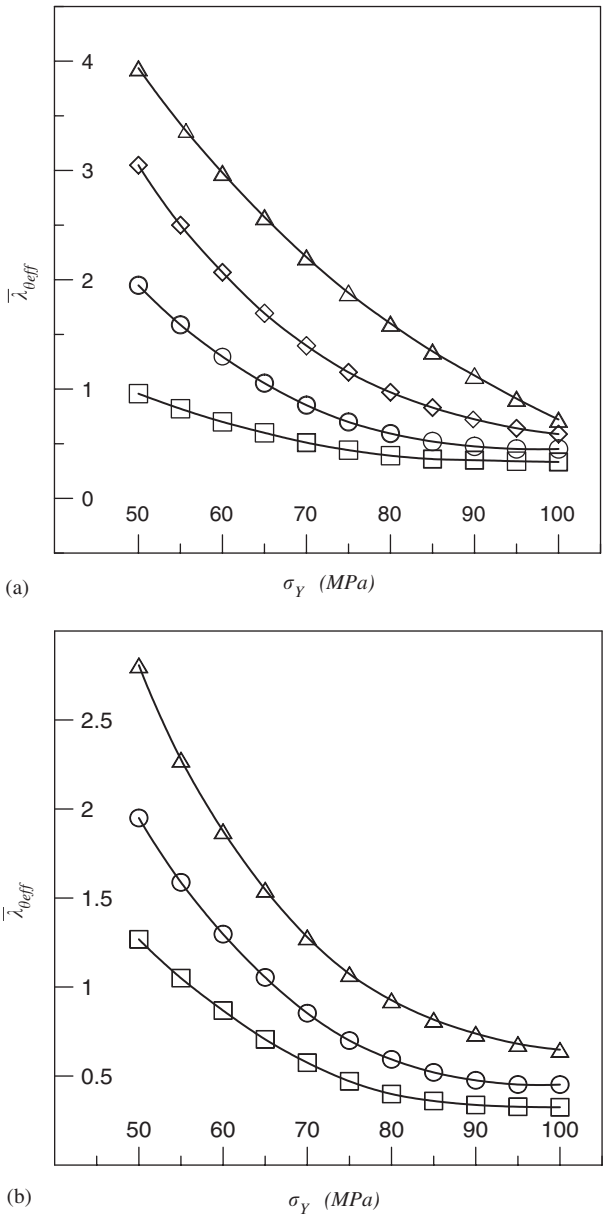

Fig. 7. Effective non-dimensional bending compliance $\bar{\lambda}_{\theta eff}$ versus yield strength for (a) four values of the applied moment per unit thickness [$\bar{M} = 0.75$ □, 1.00 ○, 1.25 ◇, 1.50 △ (kN)] at fixed crack length to depth ratio $a/d = 0.46$, and (b) three values of crack length to depth ratio [$a/d = 0.42$ □, 0.46 ○, 0.45 ◇] at fixed applied moment per unit thickness, $\bar{M} = 1.0$ kN.

the fixed beam depth $d = 1.25$ cm, the non-dimensional *elastic* compliances depend only on a/d and d/L and the rectangular shape of the cross-section of the beam and they may be found by an analysis as in Yokoyama or by using the present BEM model with a bonded ligament instead of a

Table 1
Values of elastic effective compliances

	$a/d = 0.42$	$a/d = 0.46$	$a/d = 0.50$
$(\bar{\lambda}_W)_{\text{elastic}}$	3.6763×10^{-5}	5.0008×10^{-5}	6.6390×10^{-5}
$(\bar{\lambda}_\theta)_{\text{elastic}}$	0.18885	0.24123	0.30748

Table 2
Values of first and third elastic non-dimensional wavenumbers

	$a/d = 0.42$	$a/d = 0.46$	$a/d = 0.50$
$(\kappa_1)_{\text{elastic}}$	2.8989	2.8460	2.7853
$(\kappa_3)_{\text{elastic}}$	8.8515	8.75911	8.6641

cohesive zone. The present BEM formulation was verified for the elastic case by comparing to Yokoyama's roots for a few cases. For the a/d and $d/L = 0.1$ used in this study the elastic non-dimensional compliances are given in Table 1.

Call the roots of the frequency equation (13) κ_n ($n = 1, 2, 3, \ldots$). They are related to the nth natural frequency by Eq. (10), which gives

$$\omega_n = \frac{(\kappa_n)^2}{L^2}\sqrt{\frac{EI}{\rho A}}. \tag{20}$$

The natural frequencies for the *plastic mode I* problem reported in Figs. 8a–d are normalized with respect to the *elastic* natural frequencies, i.e. values of the ratio given by

$$\frac{(\omega_n)_{\text{plastic}}}{(\omega_n)_{\text{elastic}}} = \frac{(\kappa_n)^2_{\text{plastic}}}{(\kappa_n)^2_{\text{elastic}}} \tag{21}$$

are reported. The first and third elastic roots are found using the elastic compliances in Table 1 and are independent of the crack plane load and are given in Table 2. As a further reference, from classical beam vibration analysis, the well known *uncracked* values of κ_n are equal to $n\pi$ and are obviously independent of both a/d and d/L. As a result of the increasing compliance, for a given geometry the roots always obey the inequality given below.

$$(\kappa_n)_{\text{uncracked}} > (\kappa_n)_{\text{elastic}} > (\kappa_n)_{\text{plastic}} \Leftrightarrow (\omega_n)_{\text{uncracked}} > (\omega_n)_{\text{elastic}} > (\omega_n)_{\text{plastic}}. \tag{22}$$

Note that for the present case of the crack located at the midspan, since the second mode is anti-symmetric about the midspan, the crack plane is subjected only to shear and the second mode frequency does not depend on the plastic effective bending compliance, but depends only on the elastic shear compliance $\lambda_{W\text{elastic}}$, which is independent of the static load into the nonlinear range. Hence the second mode is not sensitive to the load or the yield stress. If the crack were not located

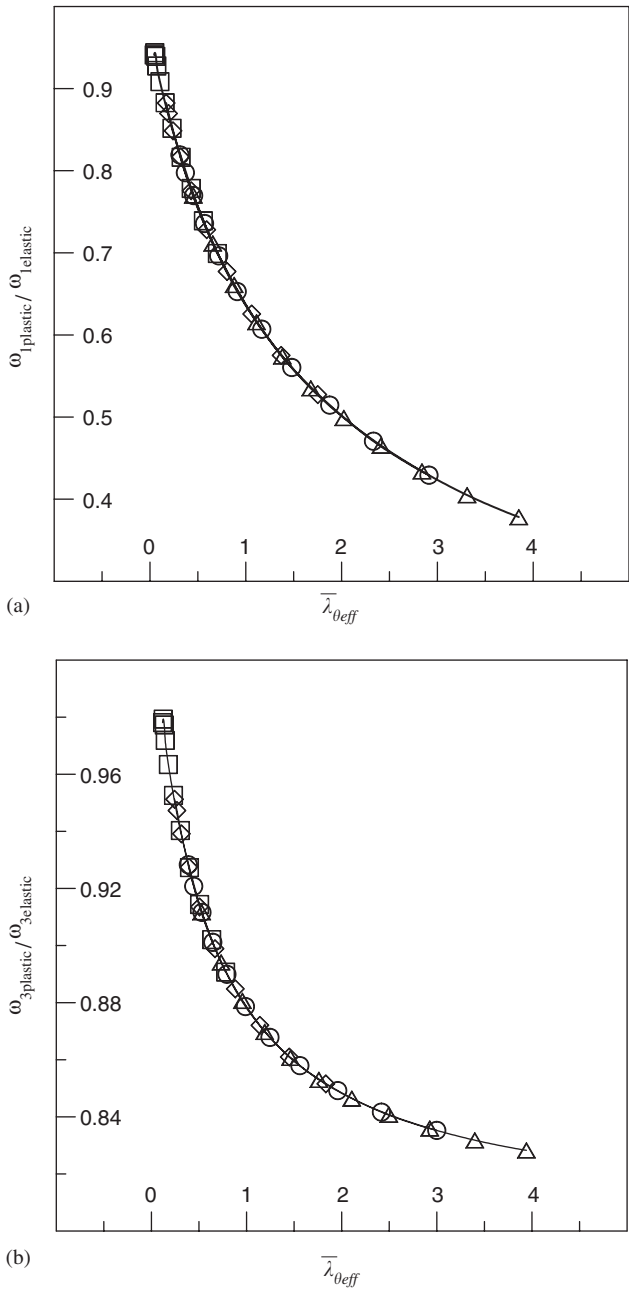

Fig. 8. Normalized frequencies versus effective non-dimensional bending compliance $\bar{\lambda}_{\theta eff}$. (a) $n = 1$. (b) $n = 3$. Symbols correspond to the data shown in Fig. 7a [$\bar{M} = 0.75$ □, 1.00 ○, 1.25 ◇, 1.50 △ (kN)] and the solid lines show the entire dependence of the frequency ratios on compliance over the entire range shown.

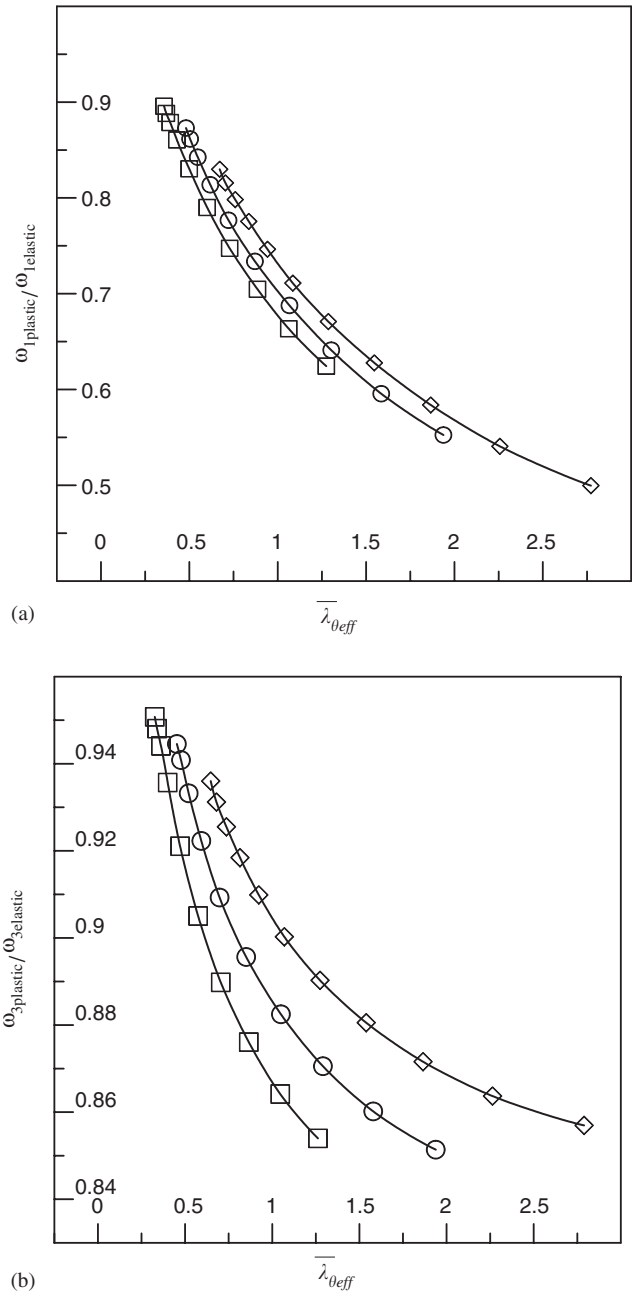

Fig. 9. Normalized frequencies versus effective non-dimensional bending compliance $\bar{\lambda}_{\theta eff}$. (a) $n = 1$ and (b) $n = 3$. Each curve corresponds to a curve in Fig. 7b at the indicated crack length to depth ratios [$a/d = 0.42$ □, 0.46 ○, 0.45 ◇].

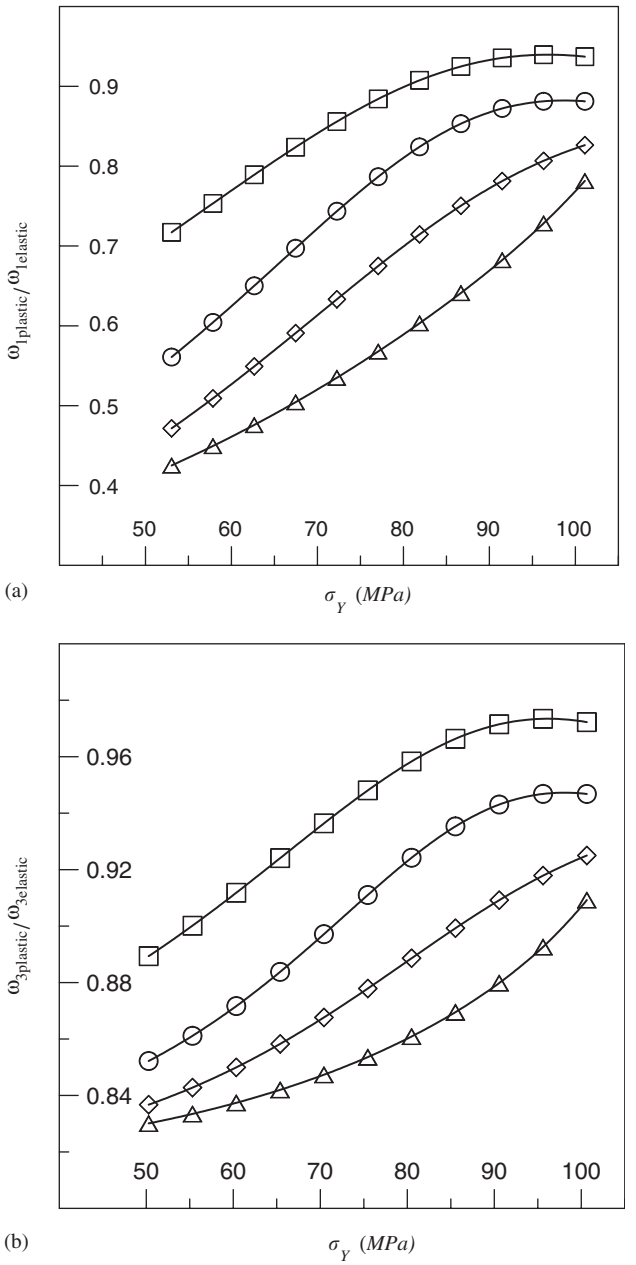

Fig. 10. Normalized frequencies versus yield stress. (a) $n = 1$. (b) $n = 3$. Each curve corresponds to a curve in Fig. 7a at the indicated applied bending moment per unit thickness [$\bar{M} = 0.75$ □, 1.00 ○, 1.25 ◇, 1.50 △ (kN)].

at the midspan all of the frequencies would depend on the nonlinear bending compliance and hence on the static nonlinear load. However, the biggest effect of the bending compliance on frequency will always occur in the first mode and when the crack is at the midspan.

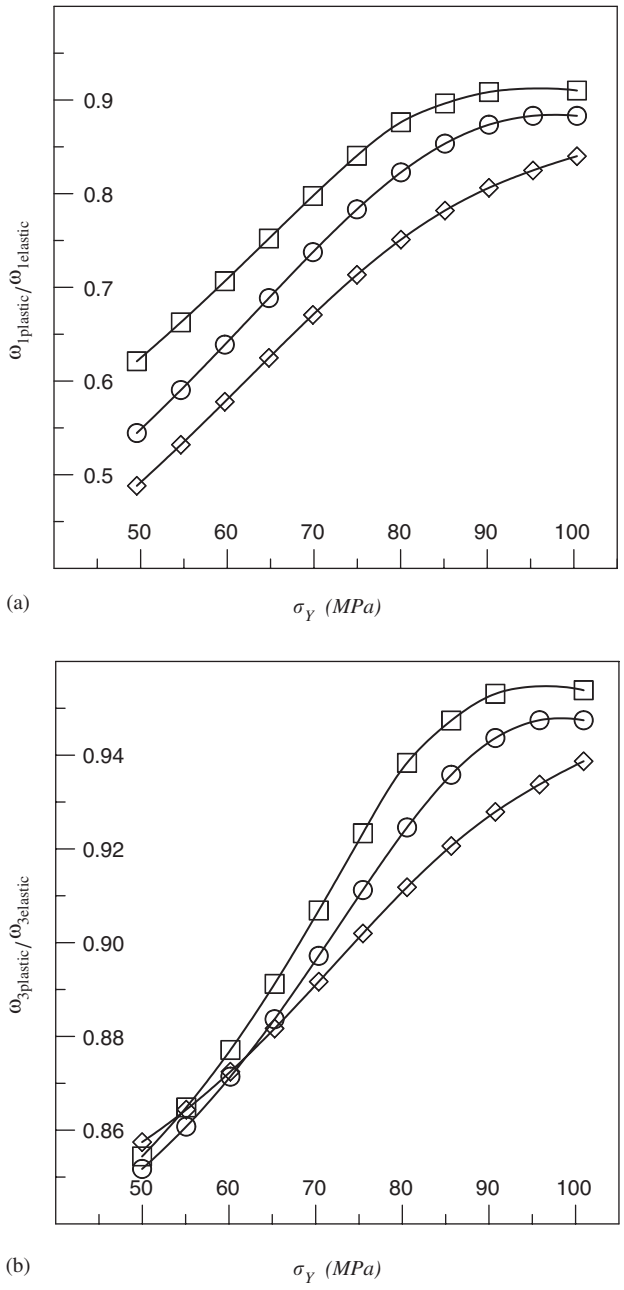

Fig. 11. Normalized frequencies versus effective yield stress. (a) $n = 1$ and (b) $n = 3$. Each curve corresponds to a curve in Fig. 7b at the indicated crack length to depth ratios [$a/d = 0.42$ □, 0.46 ○, 0.45 ◇].

Results for the $n = 1$ and $n = 3$ frequency ratios defined in Eq. (21) are shown in Figs. 8–11. Figs. 8 and 10 come from the plastic effective bending compliance curves in Fig. 7a, and Figs. 9 and 11 come from the plastic effective bending compliance curves in Fig. 7b. Figs. 8a and b show

the $n = 1$ and $n = 3$ frequency ratios versus the plastic effective bending compliance $\bar{\lambda}_{\theta\text{eff}}$ for the values of $\bar{\lambda}_{\theta\text{eff}}$ corresponding to points on the curves in Fig. 7a. The four curves in Fig. 7a are all for the same crack length and therefore map onto single master curves (solid lines) in Figs. 8a and b. This is because the elastic shear compliance is the same for all four curves in Fig. 7a at the four load levels and, hence, the frequency ratios depend only on the value of $\bar{\lambda}_{\theta\text{eff}}$ and not on the load directly. The curve in Fig. 7a from which the points come are indicated by the symbols in Figs. 7a, 8a and 8b. Note that, for example, the upper most triangle on the $M = 1.5\,\text{kN}$ curve in Fig. 7a maps to the lowest most triangle on the curves in Figs. 8a and b. Note that theoretically the effective compliance can range from zero to infinity. Each curve in Fig. 7a at successively higher loads map onto longer and longer portions of the master curve with the starting and ending point of the portion moving monotonically down the master curve. The master curves show power law behavior with very good fits out to much larger values of $\bar{\lambda}_{\theta\text{eff}}$ than shown here, decaying almost as fast as $\left(\bar{\lambda}_{\theta\text{eff}}\right)^{-1}$.

Because each of the three curves in Fig. 7b are for different crack lengths, different values of the elastic shear compliance must be used, see Table 1, and the curves map onto three different curves in Figs. 9a and b. Full master curves for the different crack lengths are not shown, nor are individual data points and the solid lines indicate the range of data in the corresponding curve in Fig. 7b. Moving left to right on each of the six curves in Figs. 9a and b, the yield stress goes from 100 MPa at the far left to 50 MPa on the far right. It can be seen that for the $n = 1$ frequency ratio in Fig. 9a that as the crack lengths increase the results are further down the curves, but the smallest slopes of each curve (at the right ends) are not too different on the three curves, indicating about equivalent amounts of saturation of the effect with respect to increasing $\bar{\lambda}_{\theta\text{eff}}$. However the results for the $n = 3$ frequency ratio in Fig. 9b the smallest slope is much less for the longer crack than for the two shorter crack lengths, indicating quite different amounts of saturation of the effect with respect to increasing $\bar{\lambda}_{\theta\text{eff}}$, saturating the fastest for the largest crack length. This causes a counterintuitive behavior in the frequency as a function of yield stress shown below.

The $n = 1$ and $n = 3$ frequency ratio vs. yield stress curves in Figs. 10a and b, respectively, correspond to the similarly marked curves in Fig. 7a, while Fig. 11 shows the frequency ratio curves which correspond to similarly marked curves in Fig. 7b. The results for different loads at a fixed crack length in Figs. 10a and b present no surprises. Frequencies increase monotonically with increasing yield stress and decreasing load as expected. The change in behavior from concave up to concave down as the load is decreased may be an exploitable identifying feature. The results for different crack lengths at a fixed load are given in Figs. 11a and b. For the entire range in Fig. 11a and most of the range in Fig. 11b the frequency ratios increase monotonically with increasing yield stress and decreasing crack length as expected, except for the $n = 3$ ratios at the lower end of the yield stress range, where the longer crack ratio does not decrease as fast as the shorter cracks with decreasing yield stress. This is a reflection of the much smaller slopes in the longer crack curve in Fig. 9b compared to the shorter cracks at low yield stress (large $\bar{\lambda}_{\theta\text{eff}}$) and indicates that the longer the crack the more quickly the compliance effect saturates as the yield decreases and there is a longer more stretched cohesive zone. This saturation could be caused by the load being so large that the cohesive zone takes over the entire ligament at a short crack length and as the crack length increases past this value the cohesive zone cannot get any longer, it just gets stretched more and more. However, care was taken that this did not occur. At the load level

in Figs. 7b, 9 and 11 the cohesive zone occupies about 90% of the ligament at the longest crack length.

7. Conclusions

It is clear from these limited calculations that the presence of a plastic cohesive zone may reduce the fundamental frequency from its value for the elastic crack without a cohesive zone by as much as 50% for low yield stress and large cohesive zones. Moreover there is relatively strong sensitivity to the yield stress over a relatively small range of only 50–100 MPa, which should be exploitable. There are two kinds of material characterization problems for which an analysis of the type presented here could be used. The first deals with determining the cohesive strength of a very thin adhesive layer between two adherends, modeled by the crack plane and the material on either side. The analysis above is for the same material on either side of the crack plane but that could easily be modified. The second deals with a crack in a homogeneous ductile beam for which the present results could be used to determine the actual yield strength or flow stress in the material near the crack tip. The success of such a method would depend very much on how applicable the assumptions of a Dugdale–Barenblatt cohesive model are for the given material. In future studies more realistic cohesive models which exhibit softening before failure will be employed, and experimental capabilities will be developed for measuring frequencies and mode-shapes of cracked beams subjected to a large static load bending moment. The simplest of the softening cohesive laws would require two or three parameter estimation as opposed to the single yield stress parameter in the present work.

References

[1] P. Gudmundson, Eigenfrequency changes of structures due to cracks, notches or other geometrical changes, *Journal of the Mechanics and Physics of Solids* 30 (1982) 339–353.
[2] P. Gudmundson, The dynamic behavior of slender structures with cross-sectional cracks, *Journal of the Mechanics and Physics of Solids* 31 (1983) 329–345.
[3] G. Bamnios, A. Trochidis, Dynamic behavior of a cracked cantilevered beam, *Applied Acoustics* 45 (1995) 97–112.
[4] G. Bamnios, A. Trochidis, Mechanical impedance of a cracked cantilevered beam, *Journal of the Acoustical Society of America* 97 (1995) 3625–3635.
[5] A.D. Dimarogonas, Vibration of cracked structures: a state of the art review, *Engineering Fracture Mechanics* 55 (1996) 831–857.
[6] T.G. Chondros, A.D. Dimarogonas, Vibration of a cracked cantilevered beam, *Journal of Vibration and Acoustics—Transactions of ASME* 18 (1997) 221–228.
[7] G.D. Gounaris, C.A. Papadopoulos, Analytical and experimental identification of beam structures in air or fluid, *Computers and Structures* 65 (1997) 633–639.
[8] T.G. Chondros, A.D. Dimarogonas, J. Yao, A continuous cracked beam vibration theory, *Journal of Sound and Vibration* 215 (1998) 17–34.
[9] T. Yokoyama, M.-C. Chen, Vibration analysis of edge-cracked beams using a line-spring model, *Engineering Fracture Mechanics* 59 (1998) 403–409.
[10] E.I. Shifrin, R. Ruotolo, Natural frequencies of a beam with an arbitrary number of cracks, *Journal of Sound and Vibration* 222 (1999) 409–423.
[11] M.A. Mahmoud, M. Abu Zaid, S. Al Harashani, Numerical frequency analysis of uniform beams with a transverse crack, *Communications in Numerical Methods in Engineering* 15 (1999) 709–715.

[12] Q.S. Li, Dynamic behavior of multistep cracked beams with varying cross section, *Journal of the Acoustical Society of America* 109 (2001) 3072–3075.
[13] T.G. Chondros, The continuous crack flexibility model for crack identification, *Fatigue and Fracture of Engineering Materials and Structures* 24 (2001) 643–650.
[14] S.S. Kessler, S.M. Spearing, M.J. Atalla, C.E.S. Cesnik, C. Soutis, Damage detection in composite materials using frequency response methods, *Composites Part B—Engineering* 33 (2002) 87–95.
[15] T.G. Chondros, A.D. Dimarogonas, J. Yao, Vibration of a beam with a breathing crack, *Journal of Sound and Vibration* 239 (2001) 57–67.
[16] J.A. Brandon, E.M.O. Lopez, A.E. Stephens, Spectral indicators in structural damage identification: a case study, *Journal of Mechanical Engineering Science—Proceedings of the Institute of Mechanical Engineers Part C* 213 (1999) 411–415.
[17] A.S. Sekhar, P. Balaji Prasad, Crack identification in a cantilever beam using coupled response measurements, *Journal of Engineering for Gas Turbines and Power* 120 (1998) 775–777.
[18] R. Ruotolo, C. Surace, P. Crespo, D. Storer, Harmonic analysis of the vibrations of a cantilevered beam with a closing crack, *Computers and Structures* 61 (1996) 1057–1074.
[19] J.R. Rice, N. Levey, The part-through surface crack in an elastic plate, *Transactions of the ASME—Journal of Applied Mechanics* 39 (1972) 185–194.
[20] M.F. Kanninen, C.H. Popelar, *Advanced Fracture Mechanics*, Oxford University Press, New York, 1985.
[21] D.S. Dugdale, Yielding of steel sheets containing slits, *Journal of the Mechanics and Physics and Solids* 8 (1960) 100–104.
[22] G.I. Barenblatt, The mathematical theory of equilibrium of crack in brittle fracture, *Advances in Applied Mechanics* 7 (1962) 55–129.
[23] D.A. Mendelsohn, T.S. Gross, L.J. Young, F. Chen, R.U. Goulet, Geometry and load fixture effects in the four-point-bend mixed mode fracture specimen, *Engineering Fracture Mechanics* 68 (2001) 587–604.
[24] L.J. Young, A boundary element analysis of fracture surface interference for mixed mode loading problems with elastic or plastic crack tips, PhD Thesis, The Ohio State University, 1994.